

Seismic Attenuation in Partially Saturated Dime-shaped Cracks

HARTMUT SCHÜTT,¹ JENS KÖHLER,² OLIVER BOYD³ and HARTMUT SPETZLER^{1,4}

Abstract—We have examined the effect of surface contamination on the attenuation and stiffness of compressional seismic waves in artificial cylindrical glass cracks that are partially saturated with water. The compression of the gap perpendicularly to its plane reduces the gap volume and forces the water to redistribute within the gap (conservation of volume of an incompressible liquid). On clean surfaces, the water can flow without significant resistance across the glass. This leads to a very low and almost constant attenuation over a wide frequency range (approx. 3 mHz to 10 Hz), while the sample stiffness is constant. In the case of propanol contaminated surfaces, both the attenuation and the stiffness are considerably higher than in the clean case, and display a considerable frequency dependence. Both effects can be explained with the Restricted Meniscus Motion Model. In this model, the redistribution of the liquid in the gap first leads to a change (increase) of the contact angle. The change of the meniscus curvature results in an increase of the pressure in the liquid and thus to a stiffening of the sample. When the resistive force, that prevents the contact line from sliding along the surface, is finally overcome, the contact line starts moving across the contaminated surface. The motion against the resistive force dissipates energy and increases the attenuation. The calculated data are in good agreement for both the clean and the contaminated case; the model parameters fall in the range that was established by independent experiments (e.g. WAITE *et al.*, 1997).

Key words: Attenuation, surface contamination, partially saturated cracks, dime-shaped.

Introduction

The attenuation of seismic waves in fluid-containing rocks is dominated by processes involving the pore fluid. Interpretation of attenuation data requires an understanding of the underlying processes. Experiments on partially saturated cracks have already shown a qualitative agreement between local fluid flow models (MURPHY *et al.*, 1986) and measured data (MÖRIG *et al.*, 1997). However, this agreement in attenuation and stiffening is only valid for frequencies higher than the relaxation frequency of the local fluid flow mechanism. The experimental results of

¹ Cooperative Institute for Research in Environmental Sciences (CIRES), University of Colorado at Boulder, Campus Box 216, Boulder, CO 80309-0216, U.S.A. e-mail: schuett@colorado.edu

² BASF AG, 201/ZC, D-67056 Ludwigshafen, Germany, formerly at ¹.

³ Western Geophysical, Houston, TX 77042, U.S.A. formerly at ⁴.

⁴ Department of Geological Sciences, University of Colorado at Boulder, Campus Box 399, Boulder, CO 80309-0399, U.S.A.

MÖRIG *et al.* (1997) showed that stiffening and attenuation do not vanish below the relaxation frequency of the local fluid flow mechanism. No such stiffening and attenuation below the relaxation frequency are predicted by local fluid flow models. WAITE *et al.* (1997) have shown that the stiffening and the attenuation below the relaxation frequency of the local fluid flow mechanism are due to the deformation and the motion of the meniscus. This can be described by a numerical model that is in good agreement with the data obtained with rectangular artificial cracks. Grain to grain contacts in sandstones may resemble penny-shaped cracks (MURPHY *et al.*, 1986) or Hertzian contacts. PALMER and TRAVIOLA (1980) have shown that the viscous attenuation is strongly dependent on the aspect ratio, i.e., the ratio thickness/diameter, of the intergranular fluid disk: The larger the aspect ratio, the smaller is the attenuation.

In this paper we extend the restricted contact line motion model of WAITE *et al.* (1997) to cylindrical symmetry. The calculations for the cylindrically shaped fluid droplets are compared with attenuation and stiffness measurements on artificial glass cracks with axis-symmetric shape for two different surface conditions: A chemically cleaned and baked sample (in the following referred to as *clean* sample), and a sample that was contaminated with propanol after cleaning (*contaminated* sample). The measurements are performed with a wideband spectrometer that is described in detail in CHERRY *et al.* (1996). The aim of these experiments is to investigate the relative contribution of different absorption mechanisms (local fluid flow, contact line motion) to the total absorption of seismic waves in fluid-filled cracks under different contamination conditions. These results are vital for the understanding of the results of seismic measurements in fluid-filled porous rocks and for the development of seismic methods for the detection of subsurface contaminants.

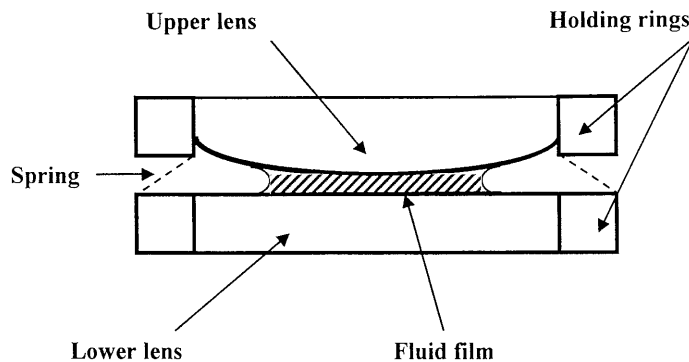


Figure 1

Basic schematic of the sample design. The curvature of the upper lens is greatly exaggerated.

Experimental Procedure

Attenuation and stiffness measurements are made using a broad band (1 mHz–100 Hz) seismic attenuation spectrometer (CHERRY *et al.*, 1996). The instrument employs an optical interferometer to measure the magnitude and the phase of the deformation of the sample and a reference. The elastic reference consists of three rectangular soda-lime glass slides separated by stainless steel wires. The sample and the reference are deformed in series. Because the reference has a stiffness near that of the sample and no measurable attenuation, the reference can be used as a stress gauge to calculate the sample's complex modulus (MÖRIG *et al.*, 1997).

The sample consists of two nearly parallel, circular glass surfaces (lenses) separated by an elastic spring (cf. Fig. 1). The upper lens is not exactly flat but slightly curved. As a result, the gap is narrowest in the center and widens towards the edges of the plates. The fluid is held in place in the center by capillary forces. The curvature of the upper lens is so low that we neglect it for the interpretation of the data, i.e., we replace the lenses by a parallel plate model. During assembly, great care is taken to achieve a reproducible stiffness of the assembly at a given gap separation. Then the gap is partially saturated with a fluid, usually water. The fluid forms a disk with cylindrical symmetry around the vertical symmetry axis of the crack (cf. Fig. 1). This configuration corresponds to the partially saturated intergranular gaps of the Murphy model (MURPHY *et al.*, 1986).

The measurements can be performed with a dry sample or with a partially saturated sample with clean or with contaminated surfaces. The clean state is achieved by heating the lenses in an oven at 420°C for 2 hours. This procedure leads to a condition which is reproducible. The clean condition is reflected in a relatively mobile fluid front when the partially saturated crack is compressed, i.e., only a small resistive force is acting against the advancing fluid. To contaminate the surfaces, the upper and lower surfaces of the gap are covered with a thin film of a fluid contaminant and are allowed to dry under room conditions. A detailed description of the experimental procedure, including the cleaning of the sample, can be found in BOYD (1997).

Restricted Meniscus Motion Model

The observation of an everyday phenomenon like sliding water drops on a vertical window can reveal much about the physics that underlie those phenomena where the contacts of different phases—solid, water, and air—play an important role. Many drops are stuck to the surface and start sliding when they grow to a critical size. The speed of the sliding drop depends on the ability of the fluid to wet the surface and on its viscous properties. The maximum size of a stuck drop is

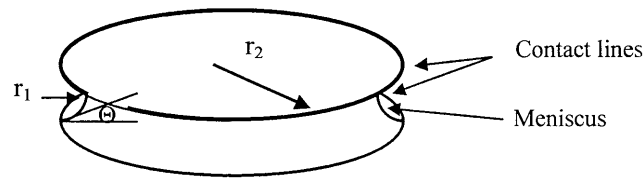


Figure 2

Schematic of the liquid disk. Θ is the contact angle, r_1 and r_2 are the radii of curvature of the meniscus ($r_1 \ll r_2$).

indicative of the maximum static forces on the line of contact. On the basis of similar observations and measurements we developed a model to explain the attenuation and dispersion of seismic waves in partially saturated media due to the existence of phase boundaries (liquid/gaseous/solid). This attenuation and dispersion occurs in addition to the effects caused by local fluid flow (MURPHY *et al.*, 1986).

The model was described in detail by WAITE *et al.* (1997). We will review here only the essentials and apply the model for the interpretation of the experimental results obtained with the cylindrical samples.

The harmonic, uniaxial compression of the sample (see Fig. 1) changes the gap volume. The fluid is assumed to be incompressible, i.e., the change in the gap height will result in a fluid redistribution. This redistribution can occur in two ways: the meniscus can change its shape and thus its contact angle and the contact lines can move across the solid surface. We assume that the meniscus retains the shape of a circular arc and that the cross section of the liquid disk between the plates is always a circle (i.e., the displacement of the contact line is independent of the azimuth).

The attenuation in this model is due to the contact line motion against a resistive force. It occurs only while the contact lines are moving. The change in the surface area of the meniscus while stuck does not contribute to the attenuation in this model. The resistive force can be found by balancing the forces (per unit length) at a stationary contact line. This balance is given by Young's equation (WAITE *et al.*, 1997):

$$\lambda_{sg} = \lambda_{sl} + \lambda_{lg} \cdot \cos \Theta_0 \quad (1)$$

λ is the surface tension at the different interfaces; the indices s , l , and g refer to the phases solid, liquid, and gas, respectively; Θ is the contact angle (cf. Fig. 3).

Optical measurements of the contact angle on oscillating plates indicate that for stationary contact lines the contact angle can vary over a range of values (WAITE *et al.*, 1997). This behavior is referred to as *contact angle hysteresis*. To allow for a range of possible contact angles, the classical Young's equation (1) must be modified:

$$\lambda_{sg} = \lambda_{sl} + \lambda_{lg} \cdot \cos \Theta + \lambda_{lg} \cdot (\cos \Theta_0 - \cos \Theta) \quad (2)$$

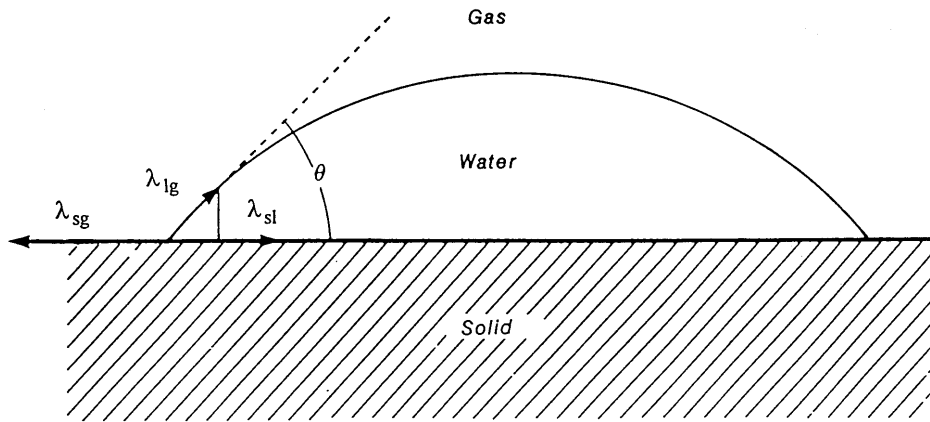


Figure 3

Contact angle Θ at a three-phase boundary, and the surface tensions between the phases (GUÉGUEN and PALCIAUSKAS, 1994).

(WAITE *et al.*, 1997).

The last term is the resistive force per unit length, and Θ_0 is the equilibrium contact angle.

Experimental data are such that the relationship between the contact angle, Θ , and the contact line velocity, v , may be represented by an equation such as

$$\Theta(v) = \Theta_0 + m \cdot v + \arctan\left(\frac{v}{v_{\text{ref}}}\right) \quad (3)$$

(WAITE *et al.*, 1997).

An example of the Θ vs. v relationship is shown in Figure 4. Equation (3) is a convenient representation of a function which is very steep around $v = 0$ but, unlike a step function, is continuous everywhere. Here m scales the slope of the curve for velocities which are large compared with the reference velocity v_{ref} , which itself scales the steepness of the curve around $v = 0$. The parameter b scales the magnitude of the hysteresis, i.e., the range of contact angle where the meniscus is stuck (cf. Fig. 4).

To calculate the behavior of the system under sinusoidal compression normal to the gap, we use an iterative approach. For every time step, the position and shape (i.e., contact angle) of the meniscus are determined using equation (3) together with the conservation of the fluid volume. As long as the meniscus can deform, the displaced liquid is accommodated in the increasing volume that is created by the bending meniscus. In this case the meniscus is stuck and the pressure in the fluid is increasing. When the meniscus can no longer deform at a rate that allows for complete accommodation of the displaced liquid, the contact line starts moving. The change of capillary pressure within the liquid is directly related to the change of the contact angle [cf. eq. (7)].

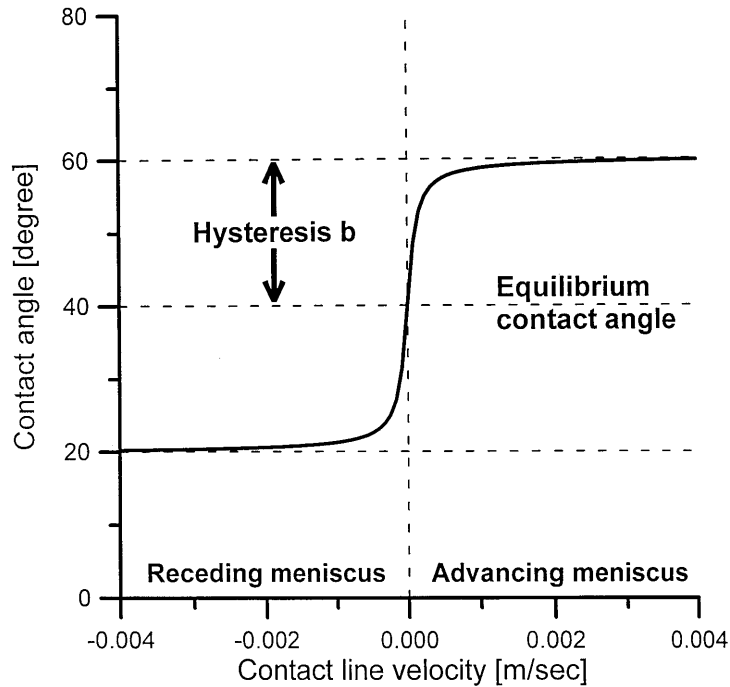


Figure 4

Contact angle as function of the contact line velocity. The hysteresis, i.e., the change of the contact angle around zero velocity, determines the nearly frequency independent portion of the total attenuation.

The force required for the deformation of the gap is due to

- (a) changes of the capillary pressure (the product of the change in capillary pressure times the wetted surface area of the gap);
- (b) the force due to the stiffness of the dry crack, i.e., a simple spring.

Energy Lost

When the force acting on the contact line exceeds the opposing resistive force F_{res} , the contact line starts sliding. The dissipated energy is simply given by force times distance, where the force is the resistive force of the sliding contact line [i.e., surface tension times total length of the two (top and bottom) contact lines $2 \cdot 2\pi r_2$ (Fig. 2)], and the distance is Δr_2 :

$$E_{\text{lost}} = \sum_{\text{cycle}} 4\pi r_2 F_{\text{res}} \Delta r = 4\pi r_2 \sum_{\text{cycle}} \lambda_{ig} [\cos \Theta_0 - \cos \Theta(v)] \Delta r. \quad (4)$$

Energy Stored

The stored energy consists of two parts:

(a) *In dry crack.* In a dry crack, the energy is stored only in the deformation of the crack as a spring (i.e., $F = k \cdot \Delta h$, where k is the spring constant and Δh is the displacement):

$$E_{\text{dry}} = \frac{1}{2} k_{\text{dry}} \Delta h_{\text{max}}^2 \quad (5)$$

where k_{dry} is the stiffness of the dry crack and Δh_{max} is the amplitude of the gap deformation.

(b) *In changes of the fluid pressure.* While the contact line is stuck, the pressure change in the liquid during deformation adds another term to the stored energy.

The capillary pressure in the liquid depends on the mean radius of the meniscus (GUÉGUEN and PALCIAUSKAS, 1994), which is given as

$$\frac{1}{r_m} = \frac{1}{r_1} + \frac{1}{r_2}. \quad (6)$$

The radii r_1 and r_2 are defined in Figure 2. (The radius of the fluid disk, r_2 , in the experiment is approximately 2 orders of magnitude larger than the radius of the meniscus, r_1 , i.e., the mean radius of the fluid-gas interface equals the meniscus radius to a good approximation.)

The increase of the capillary pressure can be calculated from Laplace's equation (e.g., GUÉGUEN and PALCIAUSKAS, 1994):

$$\Delta p_c = 2\lambda_{lg} \cdot \left(\frac{\cos \Theta_0}{h_0} - \frac{\cos \Theta}{h} \right), \quad (7)$$

where the index 0 denotes the equilibrium values of the contact angle, Θ , and of the gap height, h , respectively. The restoring force on the crack is given by the product of the capillary pressure times the wetted surface area. With the known dry stiffness of the crack, we can calculate the plate displacement, Δh_{liq} that would be caused by the capillary pressure of the liquid. Thus, the energy stored in the pressurized liquid is equivalent to the energy required to change the dry crack height by Δh_{liq} (WAITE *et al.*, 1997):

$$E_{\text{liq}} = \frac{1}{2} k_{\text{dry}} \Delta h_{\text{liq}}^2. \quad (8)$$

The total energy stored, E_{stored} , is the sum of the energy stored in the dry gap [eq. (5)] and in the liquid [eq. (8)], i.e., $E_{\text{stored}} + \frac{1}{2} k_{\text{dry}} (\Delta h_{\text{max}}^2 + \Delta h_{\text{liq}}^2)$. The attenuation is then

$$\frac{1}{Q} = \frac{1}{2\pi} \cdot \frac{E_{\text{lost}}}{E_{\text{stored}}}. \quad (9)$$

The crack stiffness is calculated from the stored energy. The restoring force is assumed to be proportional to the change of the gap separation, Δh , from the initial gap separation, h_0 ; k_{dry} is the stiffness of the dry gap, k_{wet} is the stiffness of the gap with partial fluid saturation, A is the wetted gap area.

$$\begin{aligned} E_{\text{stored}} &= \frac{1}{2} k_{\text{dry}} \Delta h_{\text{max}}^2 + \frac{1}{2} k_{\text{dry}} \left(\frac{\Delta p_c A}{k_{\text{dry}}} \right)^2 \\ &= \frac{1}{2} \left[k_{\text{dry}} \Delta h_{\text{max}}^2 + \frac{(\Delta p_c A)^2}{k_{\text{dry}}} \right] \\ &\stackrel{!}{=} \frac{1}{2} k_{\text{wet}} \Delta h_{\text{max}}^2 \end{aligned} \quad (10)$$

$$\Rightarrow \frac{k_{\text{wet}}}{k_{\text{dry}}} = 1 + \left(\frac{\Delta p_c A}{k_{\text{dry}} \Delta h_{\text{max}}} \right)^2. \quad (11)$$

Equation (11) shows that the stiffness of the partially saturated gap is higher than the stiffness of the dry gap.

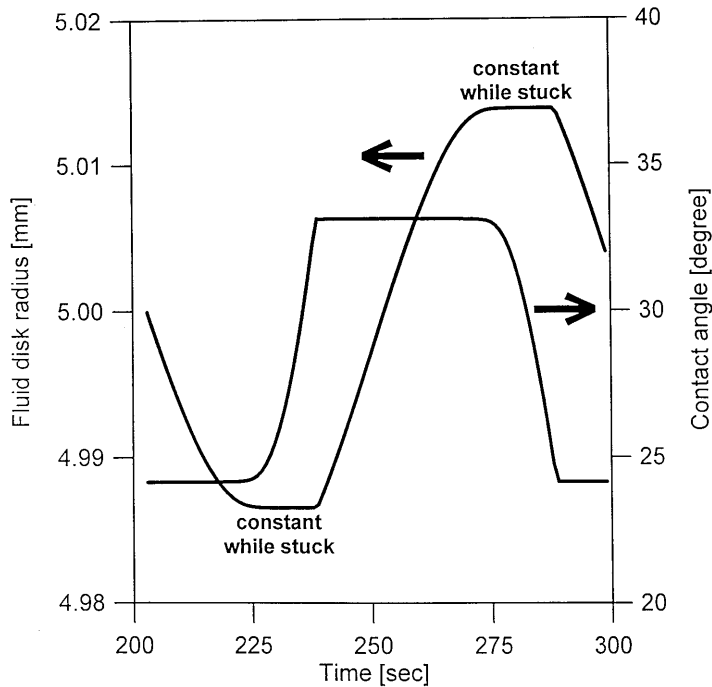


Figure 5

Fluid disk radius and contact angle for the 3rd cycle of a harmonic uniaxial compression of the fluid filled gap with 0.01 Hz. The time intervals with sliding and stuck meniscus can clearly be distinguished.

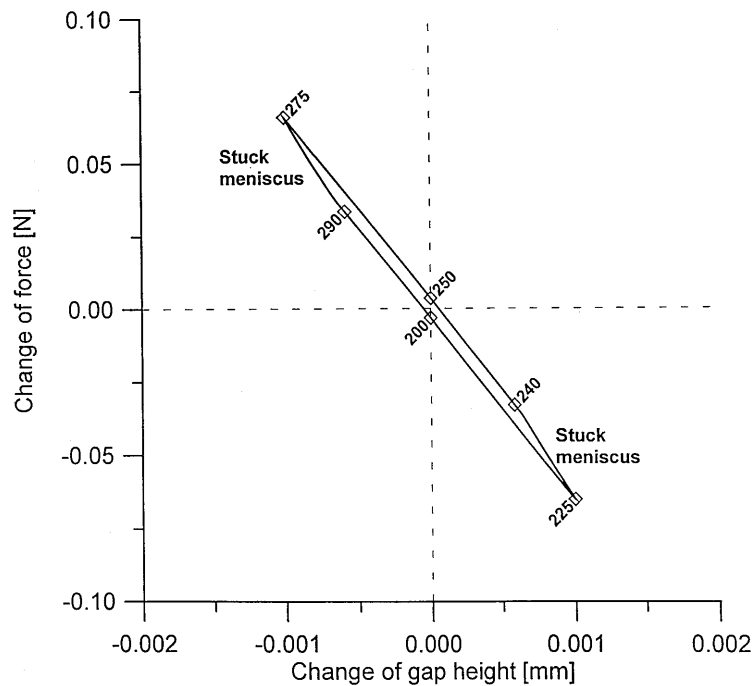


Figure 6

Hysteresis loop for the 3rd cycle of the compression at 0.01 Hz. The labels indicate the time in seconds. The parts of the curve which correspond to a stuck meniscus can be distinguished by their steeper slope. The effective stiffness of the gap over the entire cycle equals the slope of the long axis of the loop. The nonelliptical shape of the loop indicates a nonlinear behavior of the sample.

The behavior of the meniscus during one cycle of the sinusoidal deformation is shown in Figure 5. The radius of the liquid disk and the contact angle are plotted versus time. The frequency in this example is 0.01 Hz. The results are shown for the 3rd cycle, i.e., for a time interval from 200 to 300 seconds, because the modeling program requires a couple of cycles to reach a stable solution.

The sliding meniscus (changing radius) can clearly be distinguished from the stuck meniscus (constant radius) in Figure 5. In the first case, the contact angle is constant. In the latter case it is changing to accommodate the displaced liquid. From the radius vs. time graph we can easily calculate the contact line velocity. In Figure 6, the force vs. gap height relationship for a complete cycle is shown. The force is the product of the change of the fluid pressure due to the change of the contact angle [eq. (7)] and the wetted gap area. This curve can be regarded as a representation of the classical hysteresis loop, i.e., the stress-strain-behavior for a complete cycle. Unlike the classical elliptical hysteresis loop for linear systems, we obtain a loop which indicates a highly nonlinear system. This nonlinearity is a consequence of the strong amplitude dependence and is in stark contrast to other

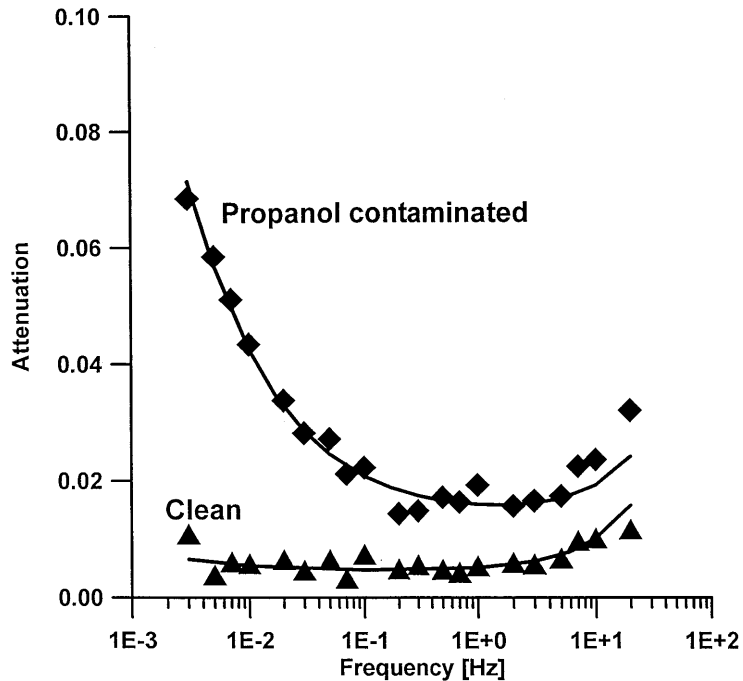


Figure 7

Frequency dependence of the attenuation in water-filled gaps for clean and propanol contaminated surfaces. Symbols are measured values, lines are results of model calculations.

models, e.g., the Murphy model (MURPHY *et al.*, 1986), that do not depend on the deformation amplitudes. The stuck meniscus (between 225 and 240 sec, and between 275 and 290 sec) can be clearly distinguished (cf. Fig. 5) from the sliding meniscus by the change of the local slopes of the curves. The area within the loop corresponds to the dissipated energy per cycle.

Results

Figures 7 and 8 illustrate the measured attenuation and stiffness as a function of frequency for both a clean sample (triangles) and a sample that was contaminated with propanol (diamonds). The saturant was distilled water in both cases. The lines are the results of numerical calculations using the restricted meniscus motion model. The model parameters are summarized in Tables 1 and 2.

The modeled attenuation data fit the measured data generally very well, only the steep increase for the contaminated sample could not be reproduced with reasonable model parameters. The modeled stiffness data that correspond to the modeled attenuation data reproduce the measured stiffnesses well for frequencies below 10

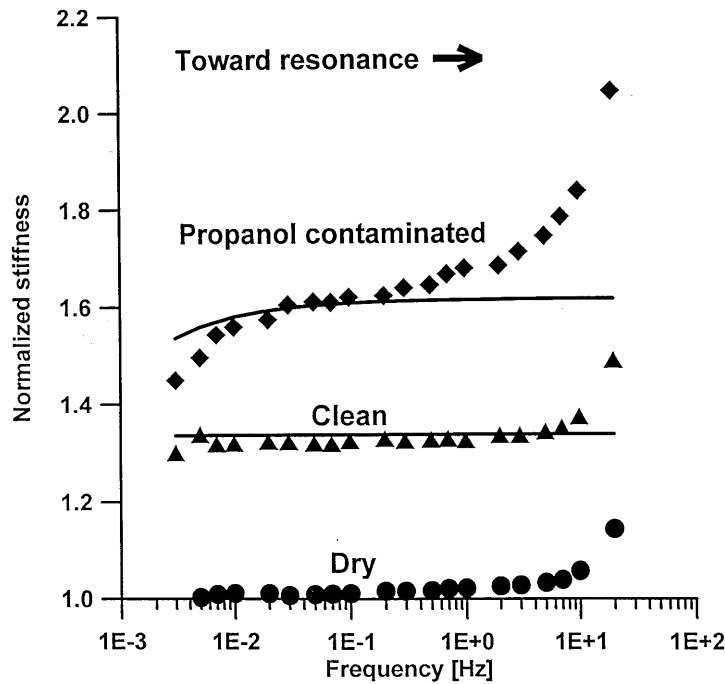


Figure 8

Frequency dependence of the stiffness corresponding to the attenuation shown in Figure 7. The increase of the stiffness at the highest frequencies might be due to resonance effects within the samples.

Hz in the case of the clean sample and for frequencies below 1 Hz in the case of the contaminated sample (the stiffness is somewhat overestimated for this sample at very low frequencies). Above these frequency thresholds the measured data manifest a pronounced increase that does not correspond to the model output. The measured stiffness of a dry sample exhibits the same behavior. Local fluid flow effects (MURPHY *et al.*, 1986) can thus be excluded. They contribute significantly only at frequencies which are at least one order of magnitude higher than those used in the experiment. We attribute the increasing stiffness at the high frequency end of the spectrum, at least in part, to apparatus resonance. The resonance frequency and peak width are themselves functions of the stiffness and attenuation. We have not included apparatus resonance in our present model.

Table 1

Constant model parameters

Gap separation	123.0 μm
Amplitude of compression	1.0 μm
Radius of fluid disk	1.0 cm
Surface tension of water	72.0 mN/m

Table 2

Physico-chemical parameters

Surface condition	θ_0 [°]	b [°]	m [°/(m/sec)]	v_{ref} [m/sec]
Clean	28.65	11.46	28.65	$2 \cdot 10^{-9}$
Contaminated	28.65	19.19	57.30	$14 \cdot 10^{-9}$

Three model parameters are particularly important to describe the attenuation and stiffness of the artificial crack in our model. The hysteresis b (see Fig. 4), which describes the change of the contact angle from its equilibrium value to the value when the meniscus finally starts moving, scales the “background” of the attenuation and stiffness. It is a problem to fit the measured data by varying b alone, since a variation of the hysteresis has two opposite effects: A large value of b means a large change of the contact angle and a large increase of the stiffness. On the other hand, a large change of the contact angle means that a large amount of the displaced fluid volume can be accommodated by the deforming meniscus. In this case, the contact line is forced to move only a very short distance or even stays at its initial position. Therefore the attenuation, which depends on the product of force (given by the change in contact angle) and contact line displacement, reacts very sensitively to a change of the geometrical parameters of the system (initial gap height, fluid disk radius, deformation amplitude): Even in the case of a high force acting on the contact line, i.e., large contact line hysteresis, the attenuation may be very small, since the contact line displacement may be very small (or zero). As a consequence, there is no simple relationship between attenuation and stiffening of the system: A very large increase of the stiffness relative to its quasistatic value is not necessarily accompanied by a high attenuation. This raises the question of causality of the model. One way to couple a high stiffening with a higher attenuation is to make the deformation of the meniscus dissipative. In our present model, energy is consumed only in the case of a moving contact line, and no energy is consumed due to the deformation of the meniscus itself. We have not yet examined whether the deformation of the meniscus with stuck contact lines dissipates energy.

The second parameter that is essential for the numerical results is the reference velocity v_{ref} which scales the slope of the contact angle vs. contact line velocity curve at very low velocities (see Fig. 4). This parameter is responsible for the attenuation and dispersion at the lower frequencies. The magnitude of both quantities depends very sensitively on v_{ref} . The significance of this result is not yet clear. The reference velocity was introduced to scale the steepness of the contact angle vs. contact line velocity curve for very low velocities, i.e., while the contact line is stuck. We model this curve as an arc tangent [eq. (3)] for its mathematical simplicity. To approach a steplike function, we had to introduce v_{ref} as a scaling

parameter with very low values. Even in the case of the contaminated sample, the curve is still very steep, although considerably less steep compared to the clean case. The most characteristic feature of the measured attenuation for the contaminated sample, the strong attenuation and dispersion at very low frequencies, can be explained only with a significant increase of v_{ref} relative to the clean case.

The modeling results also depend rather sensitively on m , the slope of the $\Theta(v)$ curve for higher velocities, but to a lesser extent than on the other two parameters. The slope m has an effect on the attenuation and stiffening at higher frequencies, but with reasonable values it is not possible to obtain a stiffening comparable to the measured increase of the stiffness. That is why we think that this stiffening is—at least in part—due to resonance effects in the samples.

The results depend only slightly on the equilibrium contact angle Θ_0 . This might be surprising because one may expect a change of the surface conditions from the clean to the contaminated sample, which should lead to different equilibrium contact angles. However, this result is consistent with the findings of WAITE *et al.* (1997). They measured angles of 22.0° for clean surfaces and 21.5° for propanol contaminated surfaces. In summary, the results of the attenuation and stiffness measurements with an artificial cylindrical model crack show distinct differences for clean and a propanol contaminated samples. In order to explain these experimental findings with a restricted meniscus motion model we must assume a larger hysteresis of the contact angle for the contaminated sample, compared to the clean case and a less steep contact angle vs. contact line velocity curve for very low velocities. Frequency dependent effects above 1 Hz are attributed to the mechanical resonance of the apparatus. Local fluid flow effects seem to be insignificant in the frequency range under consideration (3 mHz to 20 Hz).

Summary and Conclusions

In this paper we present a restricted contact line motion model to explain the measured attenuation and stiffness data from artificial circular cracks partially filled with water. Such cracks serve as a model for typical pores in natural rocks. The results from laboratory measurements on cracks with different surface contamination conditions (clean and contaminated with propanol) can be quantitatively understood when our model is applied. The model parameters fall within the range of values for meniscus behavior that have been measured independently. The clean sample displays an almost constant attenuation and stiffness for frequencies below 10 Hz. The stiffening above this threshold cannot be explained by fluid flow effects, neither contact line effects nor local fluid flow effects. It is related to the resonance when the frequency approaches the natural resonance frequency of the system. Note that the increase in stiffness is also present for the case of the dry sample, where no fluid is involved. In the case of propanol contaminated surfaces, both the

attenuation and stiffness increase considerably with increasing frequency. This increase, starting at a lower frequency for the contaminated crack, is at least qualitatively expected from the broadening of the resonance peak, which accompanies the higher attenuation.

The very high attenuation at low frequencies for the contaminated sample, which is accompanied by an increasing stiffness, is the most striking feature of the measured data. This attenuation and dispersion can be explained by the restricted meniscus motion model only by a modification of the contact angle vs. contact line velocity curve (Fig. 4) relative to the clean case. For the contaminated sample, this curve must be considerably less steep around zero velocity. The overall increase of the attenuation and stiffness from the clean to the contaminated sample can be attributed to an increase of the contact line hysteresis near zero velocity. This is in agreement with hysteresis measurements by WAITE *et al.* (1997). The model results depend very sensitively on the geometry of the crack and the fluid disk and on the deformation amplitude. The relation of the modeled attenuation and stiffness raises the question of causality, which cannot yet be answered.

REFERENCES

- BOYD, O. (1997), *Effects on Seismic Absorption due to Changed Pore Surface Properties Resulting from Exposure to Propanol: A Study Using Artificial Glass Cracks*, M.Sc. Thesis, University of Colorado at Boulder.
- CHERRY, R., SPETZLER, H., and PAFFENHOLZ, J. (1996), *A New Wideband [1 mHz to 100 Hz] Seismic Spectrometer*, *Rev. Sci. Instrum.* 67, 215–221.
- GUÉGUEN, Y., and PALCIAUSKAS, V., *Introduction to the Physics of Rocks* (Princeton University, Princeton 1994).
- MÖRIG, R., WAITE, W., and SPETZLER, H. (1997), *Effects of Surface Contamination on Fluid Flow*, *Geophys. Res. Lett.* 24, 755–758.
- MURPHY, W. F., WINKLER, K. W., and KLEINBERG, R. L. (1986), *Acoustic Relaxation in Sedimentary Rocks: Dependence on Grain Contacts and Fluid Saturation*, *Geophys.* 51, 757–766.
- PALMER, I. D., and TRAVIOLA, M. L. (1980), *Attenuation by Squirr Flow in Undersaturated Gas Sands*, *Geophys.* 45, 1780–1792.
- WAITE, W., MÖRIG, R., and SPETZLER, H. (1997), *Seismic Attenuation in a Partially Saturated Artificial Crack due to Restricted Contact Line Motion*, *Geophys. Res. Lett.* 24, 3309–3312.

(Received January 14, 1999, accepted June 2, 1999)